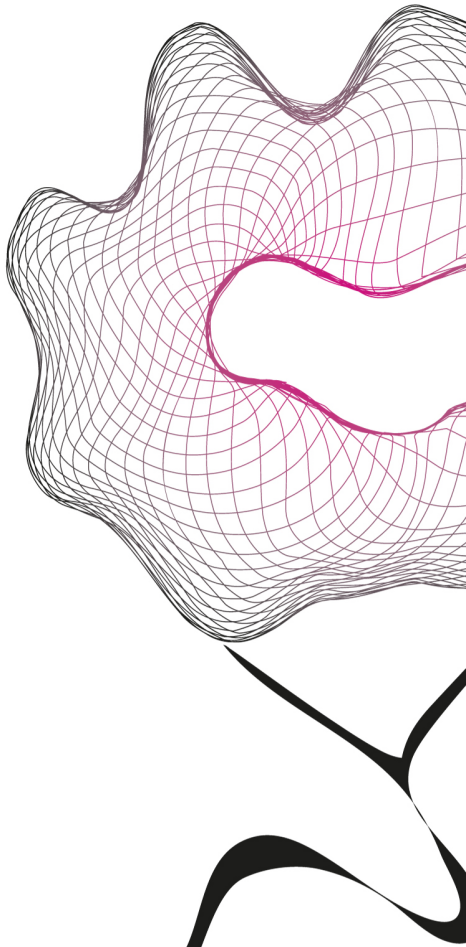


MASTER THESIS



**NEURAL FIELD STUDIES:
(I) A PITCHFORK-HOPF
BIFURCATION
(II) RELATION TO SPIKING
NEURON MODELS**

Koen Dijkstra

APPLIED MATHEMATICS
APPLIED ANALYSIS AND MATHEMATICAL PHYSICS

EXAMINATION COMMITTEE
Prof.dr. S.A. van Gils
Prof.dr. I.A. Kuznetsov
Prof.dr.ir. M.J.A.M. van Putten

Contents

1. Introduction	5
I. A pitchfork-Hopf bifurcation	7
2. Preliminaries	8
2.1. \mathbb{Z}_2 symmetries	8
3. Numerical bifurcation analysis	10
3.1. Discretization	10
3.2. Pitchfork bifurcation of the background state	10
3.3. Hopf bifurcations	11
3.4. Pitchfork-Hopf bifurcation	13
4. The normal form	14
4.1. Existence and bifurcation of fixed points	15
4.2. Bifurcation sets and phase portraits	17
5. Analytic results	18
II. Relation to spiking neuron models	20
6. A spiking neuron network	21
6.1. Spiking neuron model	21
6.2. Synaptic currents	24
6.3. Connectivity	26
7. From network to mean field	27
7.1. Averaging connectivity	27
7.2. From spikes to rates	28
7.3. Example 1: A stationary 2-bump	31
7.4. Example 2: A travelling wave	32
7.5. Example 3: A standing wave	33
8. Adding spike-frequency adaptation	34
8.1. Example 4: A moving bump	34
9. Discussion	36
References	37

1. Introduction

The most natural computational models of the brain are networks of spiking neurons. Models of individual neurons in such networks range from very detailed, biophysically realistic multi-compartment models (e.g. [20, 21]) to purely phenomenological spiking models (e.g. [13, 18, 19]). The drawback of these network models is that the very high dimensionality of parameter and state space makes them analytically untraceable and inefficient for numerical simulations.

The human brain contains roughly 100 billion (10^{11}) neurons, each making up to 1000 connections to other neurons [23]. As a result, the number of neurons and synapses in even a very small patch of brain tissue is immense. A popular approach to circumvent the problem mentioned above therefore is to take the continuum limit of a neural network in which individual spikes are replaced by a spiking rate and space is continuous. These so-called neural fields are based on the seminal work of Wilson and Cowan [24, 25], Amari [1, 2] and Nunez [16] in the 1970's and are formulated as nonlinear integral-differential equations. One modification of these original models which has received considerable attention has been the incorporation of delays [6, 12, 17]. Delays in neural networks arise due to the finite propagation velocities of action potentials along the axons, dendritic processing and synaptic mechanisms [5].

In this thesis we look at delayed neural fields of the following type

$$\left(\frac{\partial}{\partial t} + \alpha_i\right) u_i(\mathbf{r}, t) = \sum_{j=1}^p \int_{\Omega} W_{ij}(\mathbf{r}, \mathbf{r}') S_j(u_j(\mathbf{r}', t - \tau_{ij}(\mathbf{r}, \mathbf{r}')))) d\mathbf{r}' \quad (1.1)$$

for $i = 1, \dots, p$.

Equation (1.1) models $p \geq 1$ different populations of neurons distributed over the bounded, connected and open domain $\Omega \subset \mathbb{R}^n$, $n = 1, 2, 3$. The variable $u_i(\mathbf{r}, t)$ denotes the synaptic activity of population i at position $\mathbf{r} \in \Omega$, time t and exponential decay rate α_i . The right hand side of (1.1) represents the synaptic input, with $W_{ij}(\mathbf{r}, \mathbf{r}')$ denoting the connection strength between population j at location \mathbf{r}' and population i at location \mathbf{r} . The firing rate of population i at position \mathbf{r} and time t is given by $S_i(u_i(\mathbf{r}, t))$ and the propagation delays $\tau_{ij}(\mathbf{r}, \mathbf{r}')$ measure the time it takes for a signal sent by a type- j neuron located at position \mathbf{r}' to reach a type- i neuron located at position \mathbf{r} .

Let τ_m denote the maximal delay arising in (1.1).

$$\tau_m = \sup_{\mathbf{r}, \mathbf{r}' \in \Omega} \tau(\mathbf{r}, \mathbf{r}') \quad (1.2)$$

Therefore, to solve (1.1) for $t \geq 0$, we have to prescribe an initial condition φ on the interval $-\tau_m \leq t \leq 0$.

$$u(x, t) = \varphi(x, t) \quad \text{for } t \in [-\tau_m, 0] \quad (1.3)$$

This thesis consists of two parts. In part I we look at an example of (1.1) in the most simple case $p = n = 1$. Using a discretization as in [9] and numerical bifurcation analysis, bifurcation curves are computed in section 3. A codimension two point in the discretization of (1.1) is located, where a pitchfork and a Hopf bifurcation coincide. In section 4 normal form theory is used to classify the pitchfork-Hopf bifurcation. The classification is confirmed by explicitly computing the normal form coefficients of the full model in section 5. In [22] the authors show how delayed neural fields of the form (1.1) can be cast as abstract delay differential equations. Analytic expressions for the normal form coefficients of codimension one and two bifurcations can be derived under the assumption that the firing rate function is given by a finite linear combination of exponentials. Their method is illustrated by the example of a double Hopf bifurcation in the same model as is considered in part I of this thesis.

Part II of this thesis is about the relation of the delayed neural field equation (1.1) to spiking neuron models. In general, neural fields are no reductions of large neural networks but more heuristic. Therefore, there is no direct relation between parameters in the network and the mean field model and the relation between variables in the mean field and physiologically measured quantities is unclear.

In part II we derive equation (1.1) as the deterministic spatial continuum limit of a network of spiking neurons with random connections. The underlying neuron model is a slight modification of the Rulkov model [18, 19] and given in section 6. It can replicate a wide variety of spiking patterns. However, the mean field reduction given in section 7 is only possible for non-bursting neurons. The parameter relationship is clear and simulations show that the accordance between the network and the mean field is very good. In section 8 the delayed mean field model (1.1) is altered to also incorporate spike-frequency adaptation. Neural fields which take into account spike-frequency adaptation were earlier studied in [7, 14]. In our case this modification directly follows from the underlying spiking neuron model and is therefore straightforward to implement.

As a final introductory remark I want to mention that this thesis is not as complete as I would like it to be. While working two different completely different tasks was fruitful, educational and most of all a lot of fun, it always gave me an excuse to attack a new problem instead of writing a solved one down nice and neatly. This came back to roost in the end, when I once more experienced the truth of the idiom 'the devil is in the details'.

Part I.

A Pitchfork-Hopf bifurcation in a neural field model with propagation delays

2. Preliminaries

In this part, we look at a single population model on a one-dimensional spacial domain Ω with homogeneous and isotropic connectivity. The finite propagation speed of action potentials leads to a transmission delay and due to synaptic processes there is an additional fixed, 'intrinsic' delay τ_0 . Space and time are scaled such that $\Omega = (-1, 1)$ and the propagation speed is 1. This yields

$$\left(\frac{\partial}{\partial t} + \alpha\right) u(x, t) = \int_{-1}^1 w(x-y) S(u(y, t - \tau(x-y))) dy \quad (2.1)$$

with

$$\tau(d) = \tau_0 + |d| \quad (2.2)$$

We choose the connectivity function $w(d)$ as a difference of exponentials

$$w(d) = g_e e^{-b_e |d|} - g_i e^{-b_i |d|} \quad (2.3)$$

with $g_e, g_i, b_e, b_i > 0$.

This effectively models a mixed population with local excitation (inhibition) and lateral inhibition (excitation) for $g_e > g_i, b_e > b_i$ (respectively $g_e < g_i, b_e < b_i$). See part II for a motivation of this type of connectivity.

The firing rate function $S(x)$ is given by an odd sigmoid with steepness parameter $\kappa > 0$.

$$S(x) = \frac{1}{1 + e^{-\kappa x}} - \frac{1}{2} \quad (2.4)$$

Since $S(0) = 0$, we here assume that the background activity has been subtracted so that u represents the deviation from background and (2.1) admits the trivial steady state $u = 0$, which we from now on will call background state.

2.1. \mathbb{Z}_2 symmetries

Equation (2.1) is invariant to the symmetry transformations T_1 and T_2 with respect to the spatial variable defined by

$$T_1 v(x) = v(-x) \quad (2.5)$$

$$T_2 v(x) = -v(x) \quad (2.6)$$

The second symmetry holds since S is odd. Note that the fixed-point subspace X^+ of T_1 is given by all even functions while T_1 is the central reflection on the subspace X^- given by all odd functions.

$$X^+ = \{v \mid v(x) = v(-x)\} \quad (2.7)$$

$$X^- = \{v \mid v(x) = -v(-x)\} \quad (2.8)$$

Since the fixed-point subspace of $T_3 = T_1T_2$ is given by X^- we can conclude that both X^+ and X^- are invariant subspaces of (2.1).

From Theorems 7.7 and 7.8 in [15] follows that solutions of (2.1) emerging from a bifurcation of the background state are either in X^+ or in X^- .

3. Numerical bifurcation analysis

3.1. Discretization

In [9] is explained how equations of the type (1.1) can be solved numerically. A few minor corrections are given in [22]. In the case of (2.1) the spatial domain Ω is discretized into m subintervals of equal length $h = \frac{2}{m}$, leading to a system of $m + 1$ equations with $m + 1$ fixed delays, given by

$$\frac{d}{dt}u_i(t) = -\alpha u_i(t) + h \sum_{j=1}^{m+1} a_j w(|i - j|h) S(u_j(t - \tau_0 - |i - j|h)) \quad (3.1)$$

for $i = 1, \dots, m + 1$ and

$$a_j = \begin{cases} \frac{1}{2} & \text{if } j \in \{1, m + 1\} \\ 1 & \text{otherwise} \end{cases}$$

The finite-dimensional discretization (3.1) can be solved with *dde23*, a function written in *Matlab* and analysed with *DDE-Biftool* [8], a numerical bifurcation package for *Matlab*.

In the following we use a discretization of $m = 50$ subintervals and fix the parameters $\alpha = 1$ and connectivity $w(r) = 30e^{-5r} - 15e^{-r}$ (see figure 3.1). Free parameters are κ , the steepness of the firing rate function, and the fixed delay τ_0 .

Since parameter τ_0 only influences the delays in (2.1), only the stability but neither the position (shape) nor the existence of stationary solutions depend on τ_0 .

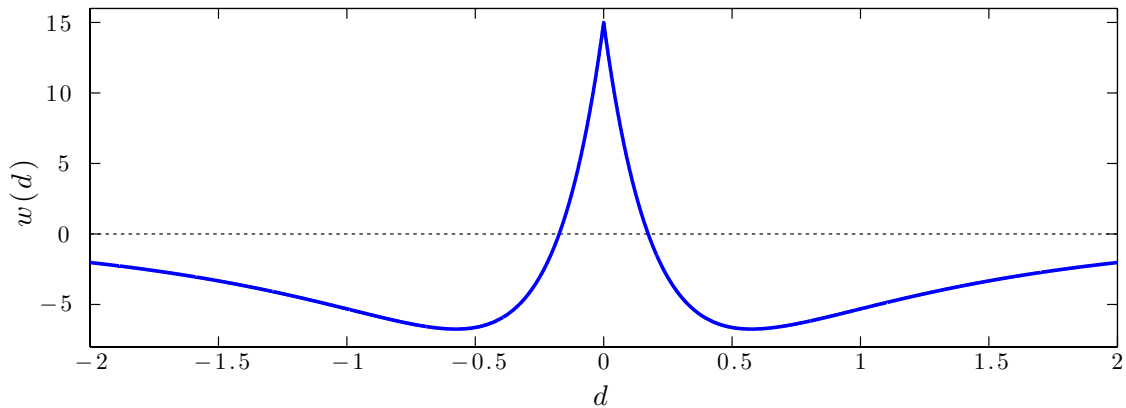


FIGURE 3.1: 'Wizard hat' connectivity function $w(d)$.

3.2. Pitchfork bifurcation of the background state

Let us first fix $\tau_0 = 1$ and consider the steepness κ of the firing rate function as the bifurcation parameter. Since $S'(0) = \frac{\kappa}{4}$ the background state is stable if κ is small enough and becomes unstable beyond some critical value κ_c . Symmetry of the system suggests that this bifurcation can be of pitchfork type. Indeed, a supercritical pitchfork bifurcation

occurs at the parameter values shown in table 3.1. For $\kappa > \kappa_c$ symmetry related stable stationary bump solutions exist. The bifurcation takes place in the even subsystem so the emerging stationary solutions are elements of X^+ . A bifurcation diagram and an example of such a bump solution are shown in figure 3.2.

TABLE 3.1: Parameter values corresponding to a pitchfork bifurcation of the background state in the discretized system ($m = 50$).

parameter	α	g_e	g_i	b_e	b_i	τ_0	κ
value	1	30	15	5	1	1	0.7740

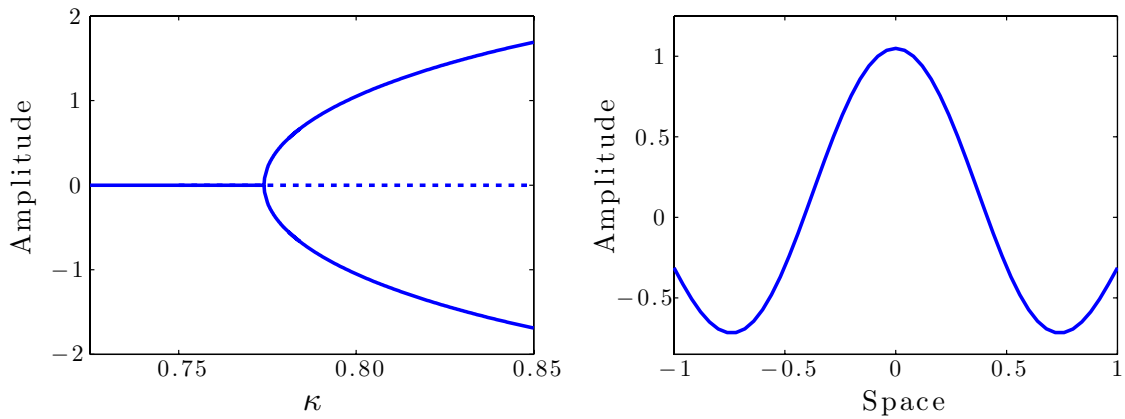


FIGURE 3.2: *Left*: Bifurcation diagram corresponding to the supercritical pitchfork bifurcation of the background state. Solid line corresponds to stable solutions, dotted line to unstable ones. Amplitude is given as the height of the bump at position $x = 0$. *Right*: Stationary bump solution for $\kappa = 0.8$ beyond the pitchfork bifurcation.

3.3. Hopf bifurcations

Hopf bifurcations play an important role in the study of neural field equations since they are the origin of oscillations, which correspond to brain waves and rhythms. Until now we have seen two types of stable solutions, the trivial background state and the stationary bumps emerging from a pitchfork bifurcation. Both these attractors can lose their stability due to a Hopf bifurcation if the intrinsic delay τ_0 is increased. Both these Hopf bifurcations lead to symmetric oscillations around the background state, see figure 3.4. The bifurcation curves are plotted in figure 3.3.

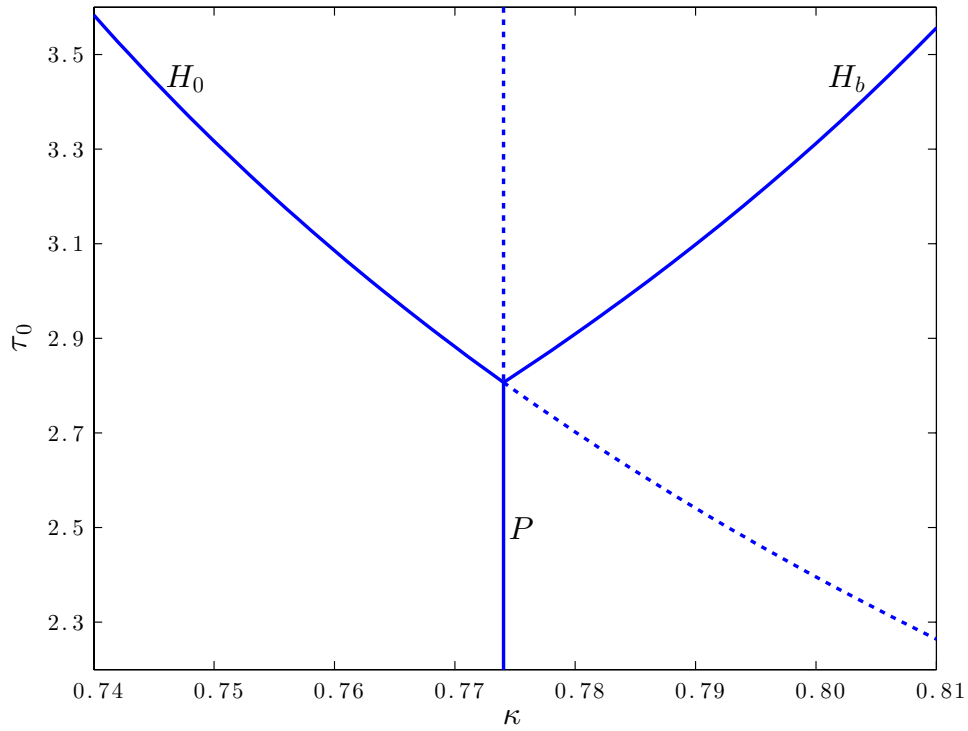


FIGURE 3.3: Bifurcation diagram. P : Pitchfork bifurcation of the background state. H_0 : Hopf bifurcation of the background state. H_b : Hopf bifurcation of bump solutions.

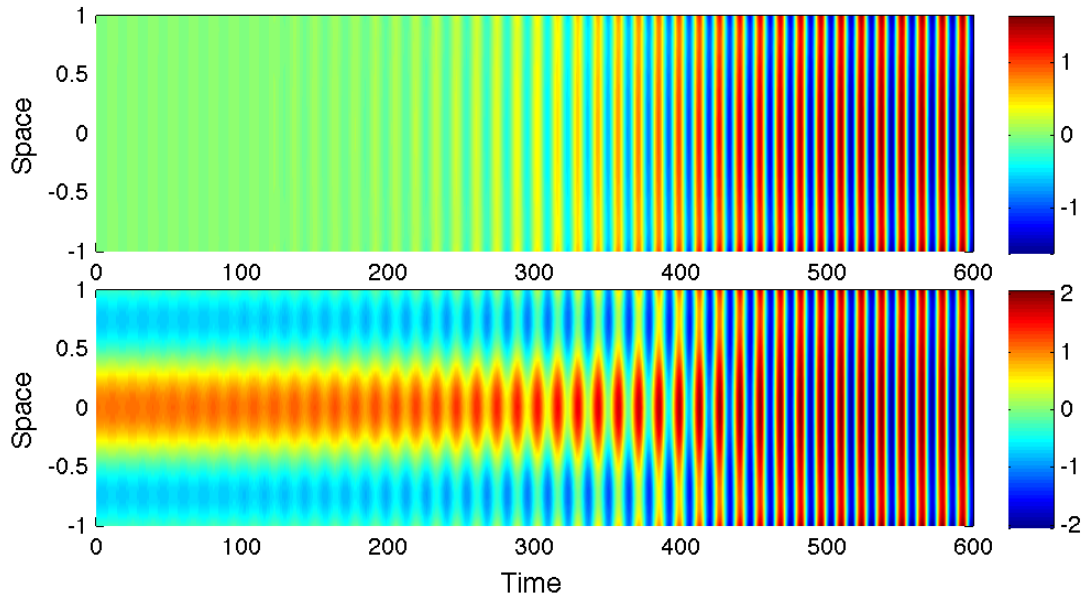


FIGURE 3.4: Simulations beyond the Hopf bifurcations of the background state and stationary bump solution. *Top* and *bottom* correspond to parameter values $(\kappa = 0.76, \tau_0 = 5)$ and $(\kappa = 0.8, \tau_0 = 5)$ respectively. Initial conditions are chosen close to the stationary states.

3.4. Pitchfork-Hopf bifurcation

As is apparent from figure 3.3 the bifurcation curves of the background state cross at a pitchfork-Hopf bifurcation. The parameter values corresponding to this critical point are given in table 3.2.

TABLE 3.2: Parameter values corresponding to a pitchfork-Hopf bifurcation of the background state in the discretized system ($m = 50$).

parameter	α	g_e	g_i	b_e	b_i	τ_0	κ
value	1	30	15	5	1	2.8068	0.7740

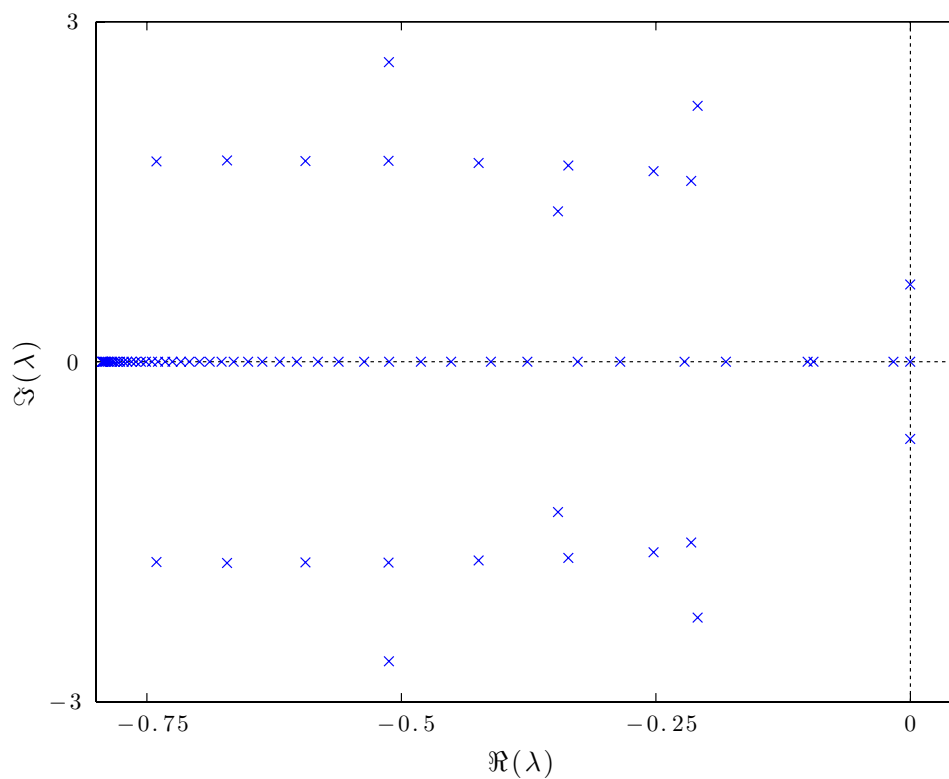


FIGURE 3.5: Spectrum at the critical point given in table 3.2. The pair of purely imaginary critical eigenvalues is given by $\lambda = \pm 0.6809i$.

4. The normal form

In [11, 15] the normal form of the pitchfork-Hopf bifurcation is given. In polar coordinates it reads

$$\begin{cases} \dot{r} = r(\mu_1 + p_{11}r^2 + p_{12}z^2) + \mathcal{O}(|r, z|^5) \\ \dot{z} = z(\mu_2 + p_{21}r^2 + p_{22}z^2) + \mathcal{O}(|r, z|^5) \\ \dot{\theta} = \omega + \mathcal{O}(|r, z|^2) \end{cases} \quad (4.1)$$

where μ_1 is the Hopf and μ_2 the pitchfork parameter. The first two equations in (4.1) are independent of the third one, which describes rotations in the plane $z = 0$. Truncating higher order terms, we can therefore restrict to the planar amplitude system

$$\begin{cases} \dot{r} = r(\mu_1 + p_{11}r^2 + p_{12}z^2) \\ \dot{z} = z(\mu_2 + p_{21}r^2 + p_{22}z^2) \end{cases} \quad (4.2)$$

where we assume that $p_{ij} \neq 0$ for $i, j \in \{1, 2\}$ and $p_{11}p_{22} - p_{12}p_{21} \neq 0$.

Since both the Hopf bifurcation and the pitchfork bifurcation of the background state are supercritical, we can conclude that $p_{11} < 0$ and $p_{22} < 0$ in our case.

The number of parameters in (4.2) can be reduced by rescaling the variables. Setting $\hat{r} = \sqrt{-p_{11}}r$, $\hat{z} = \sqrt{-p_{22}}z$ and dropping the hats leads to

$$\begin{cases} \dot{r} = r(\mu_1 - r^2 - bz^2) \\ \dot{z} = z(\mu_2 - cr^2 - z^2) \end{cases} \quad (4.3)$$

where

$$b = \frac{p_{12}}{p_{22}}, \quad c = \frac{p_{21}}{p_{11}}. \quad (4.4)$$

System (4.3) is symmetric in both r and z . Since r denotes a radius, solutions (r, z) and $(-r, z)$ of (4.3) coincide, so we can restrict to $r \geq 0$.

Following [11], the unfolding (4.2) can be classified into twelve topologically different cases. Since we already fixed the signs of p_{11} and p_{22} , six of those cases remain, see table 4.1.

TABLE 4.1: Different unfoldings of (4.3).

Case	Ia	Ib	II	III	IVa	IVb
b	+	+	+	-	-	-
c	+	+	-	+	-	-
$1 - bc$	+	-	(+)	(+)	+	-

In [15], the combined unfoldings listed in table 4.1 are called the 'simple' case', since (4.2) can not have periodic orbits for $p_{11}p_{22} > 0$.

4.1. Existence and bifurcation of fixed points

Let us now focus on the equilibria of the amplitude equations (4.3). It is clear that the trivial fixed point $(0, 0)$ exists for all values of μ_1, μ_2 and is linearly stable if both $\mu_1 < 0$ and $\mu_2 < 0$ and linearly unstable if either $\mu_1 > 0$ or $\mu_2 > 0$. Non-trivial fixed points of (4.3) can be classified in three types as shown in table 4.2 where also the corresponding solutions of the mean field equation (2.1) are given.

TABLE 4.2: Solution correspondence.

Amplitude Solution	Mean field Solution
trivial fixed point $(0, 0)$	background state
mode one fixed point $(\bar{r}, 0)$	oscillation around the background state
mode two fixed point $(0, \bar{z})$	stationary solution
mixed mode fixed point (\bar{r}, \bar{z})	oscillation around a non-trivial state

For $\mu_1 > 0$ there exists a mode one fixed point given by

$$E_1 = (\sqrt{\mu_1}, 0) \quad (4.5)$$

Linearization around this equilibrium yields eigenvalues

$$\begin{aligned} \lambda_1 &= -2\mu_1 \\ \lambda_2 &= \mu_2 - c\mu_1 \end{aligned}$$

Since we observe stable oscillations around the background state for $\kappa > \kappa_c$ in our mean field model (see figure 3.4), we can conclude that $c > 0$.

Equilibrium E_1 bifurcates on the curve

$$T_1 = \left\{ (\mu_1, \mu_2) \mid \mu_1 = \frac{1}{c}\mu_2 \text{ and } \mu_1 > 0 \right\} \quad (4.6)$$

For $c > 0$ the fixed point E_1 is an attractor if $\mu_1 > \frac{1}{c}\mu_2$ and a saddle if $\mu_1 < \frac{1}{c}\mu_2$.

For $\mu_2 > 0$ there exists a pair of mode two fixed points given by

$$E_{2,3} = (0, \pm\sqrt{\mu_2}) \quad (4.7)$$

These equilibria correspond to the bump solutions in our mean field model. Linearization around these fixed points leads to eigenvalues

$$\begin{aligned} \lambda_1 &= \mu_1 - b\mu_2 \\ \lambda_2 &= -2\mu_2 \end{aligned}$$

Therefore the bifurcation curve of the equilibria $E_{2,3}$ is given by

$$T_2 = \{(\mu_1, \mu_2) \mid \mu_1 = b\mu_2 \text{ and } \mu_2 > 0\} \quad (4.8)$$

The fixed points $E_{2,3}$ are stable as long as $\mu_1 < b\mu_2$. From figure 3.3 we can therefore deduce that $b > 0$ in our case.

Mixed mode equilibria of (4.3) are given by

$$E_{4,5} = \left(\sqrt{\frac{\mu_1 - b\mu_2}{1 - bc}}, \pm \sqrt{\frac{\mu_2 - c\mu_1}{1 - bc}} \right) \quad (4.9)$$

with bifurcation curves (4.6) and (4.8). At these curves the mixed mode fixed points coincide with a pure mode equilibrium. If $1 - bc > 0$, the mixed mode fixed points (4.9) are stable, and if $1 - bc < 0$ they are unstable. Since the Hopf bifurcation of the bump solutions is subcritical, we can conclude that $1 - bc < 0$. Therefore, we are in case Ib of [11] or, using the classification of [15], in 'simple' case I. The characteristic of this case is a bistable region in which a stationary solution and a periodic solution coexist.

In figure 3.3 this region is located beneath the Hopf bifurcation curve of the bump solutions. A simulation in this region illustrating the bistability is shown in figure 4.1. Initial conditions are given by

$$u(x, t) = \epsilon \cos(\pi x) \quad (4.10a)$$

$$u(x, t) = \epsilon \quad (4.10b)$$

for $\epsilon = 0.01$ and $t \in [-(\tau_0 + 2), 0]$.

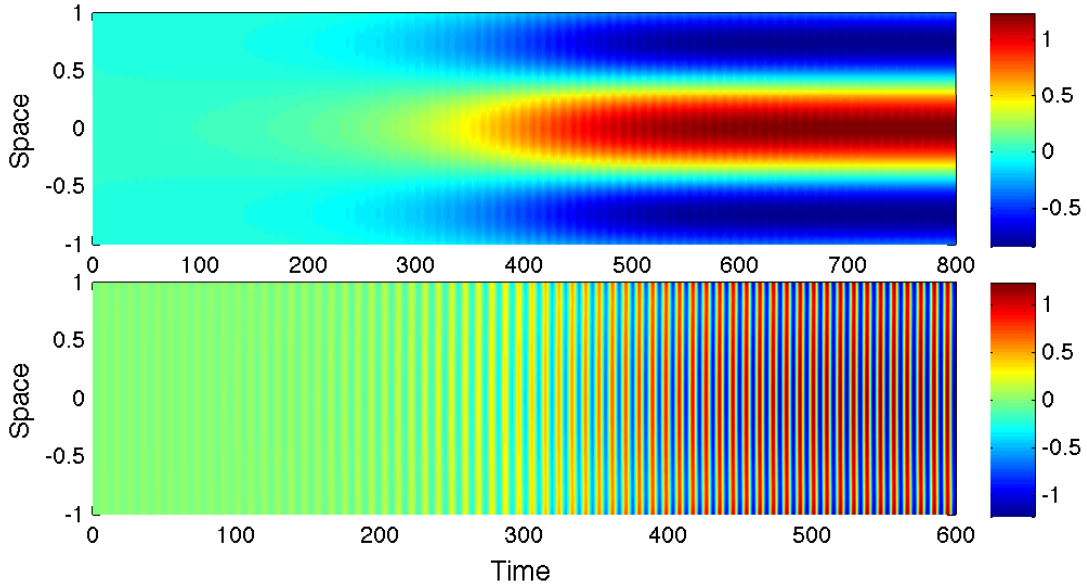


FIGURE 4.1: Bistability for $(\kappa = 0.81, \tau_0 = 2.9)$. *Top* and *bottom* correspond to initial conditions (4.10a) and (4.10b) respectively.

4.2. Bifurcation sets and phase portraits

Figure 4.2 shows the bifurcation sets and phase portraits of unfolding Ib.

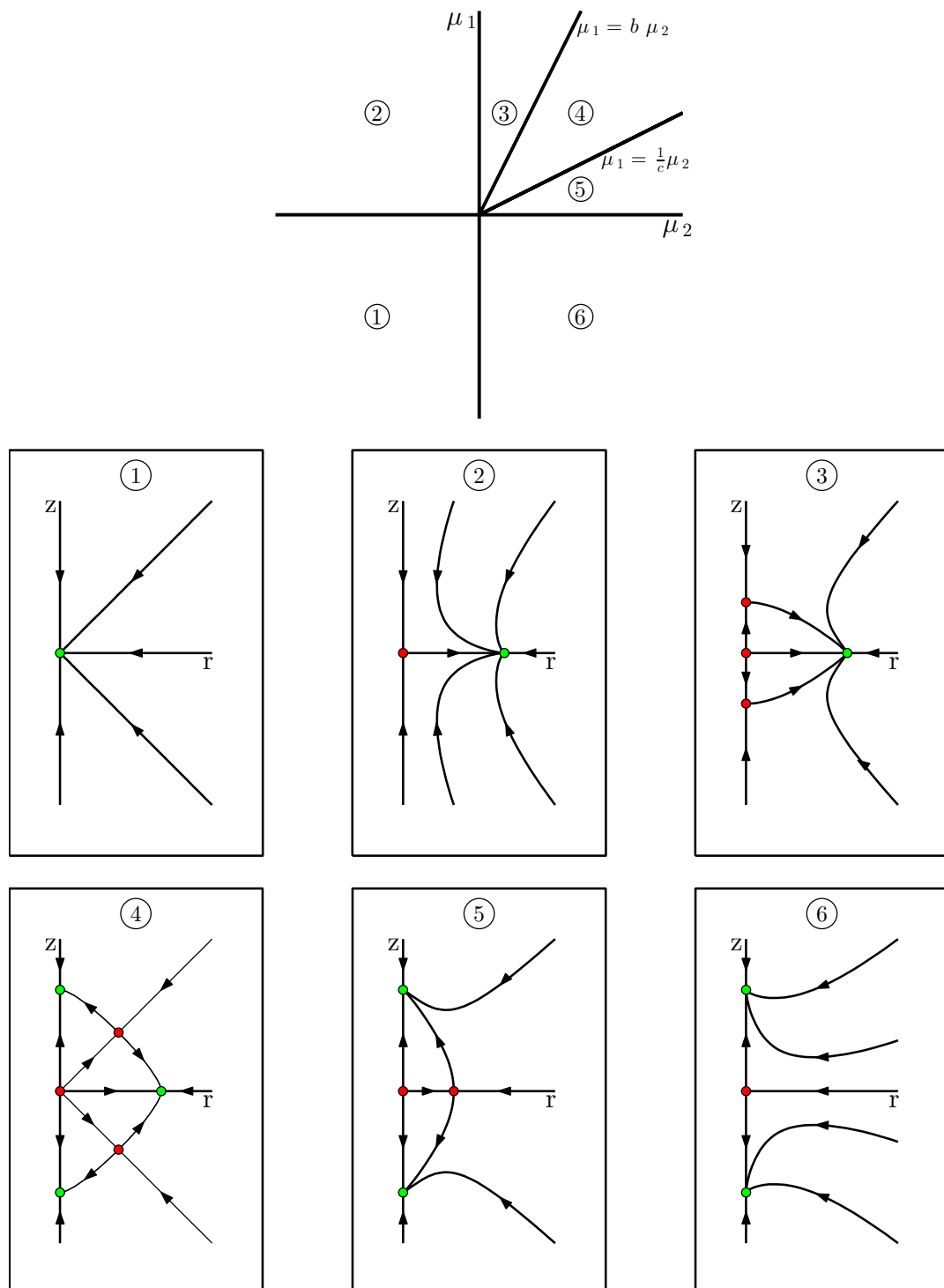


FIGURE 4.2: Case Ib.

5. Analytic results

In the recent paper [22], the authors explain how neural fields of the type (1.1) can be cast as abstract delay differential equations. Under the assumption that the firing rate function is a finite linear combination of exponentials, they derive analytic formulas for the location of the eigenvalues, the eigenfunctions and critical normal form coefficients. This enables us to verify our numerical findings in section 3 and the classification of the pitchfork-Hopf bifurcation in section 4 by numerically solving these analytic expressions. We start by calculating the critical codimension-two point of the full system (2.1), given in table 5.1.

TABLE 5.1: Parameters corresponding to a pitchfork-Hopf bifurcation of the background state in the full system (2.1).

parameter	α	g_e	g_i	b_e	b_i	τ_0	κ
value	1	30	15	5	1	2.6122	0.7791

Comparing these findings to the values in table 3.2 shows that the error in the discretization with $m = 50$ is much larger than in the example given in [22]. This can be explained by our choice of the connectivity (2.3). The greater decay translates into a bigger error in the discretized system. Nevertheless, the agreement of the critical eigenvalues and eigenfunctions is very good, as illustrated in figures 5.1 and 5.2. The stationary bump solutions are well approximated by the eigenfunction ϕ_1 corresponding to the zero eigenvalue, while the period and shape of the oscillation around the background state in figure 4.1 is well approximated by the critical eigenvalue $\lambda = 0.7062i$ and eigenfunction ϕ_2 .

We conclude this section with the normal form coefficients. They are given by

$$\begin{bmatrix} p_{11} & p_{12} \\ p_{21} & p_{22} \end{bmatrix} = \begin{bmatrix} -0.0197 & -0.1371 \\ -0.0423 & -0.1134 \end{bmatrix} \quad (5.1)$$

We indeed have $p_{11} < 0$, $p_{22} < 0$, $b = \frac{p_{12}}{p_{22}} \approx 1.21 > 0$, $c = \frac{p_{21}}{p_{11}} \approx 2.15 > 0$ and therefore $bc > 1$, which verifies our findings in section 4.

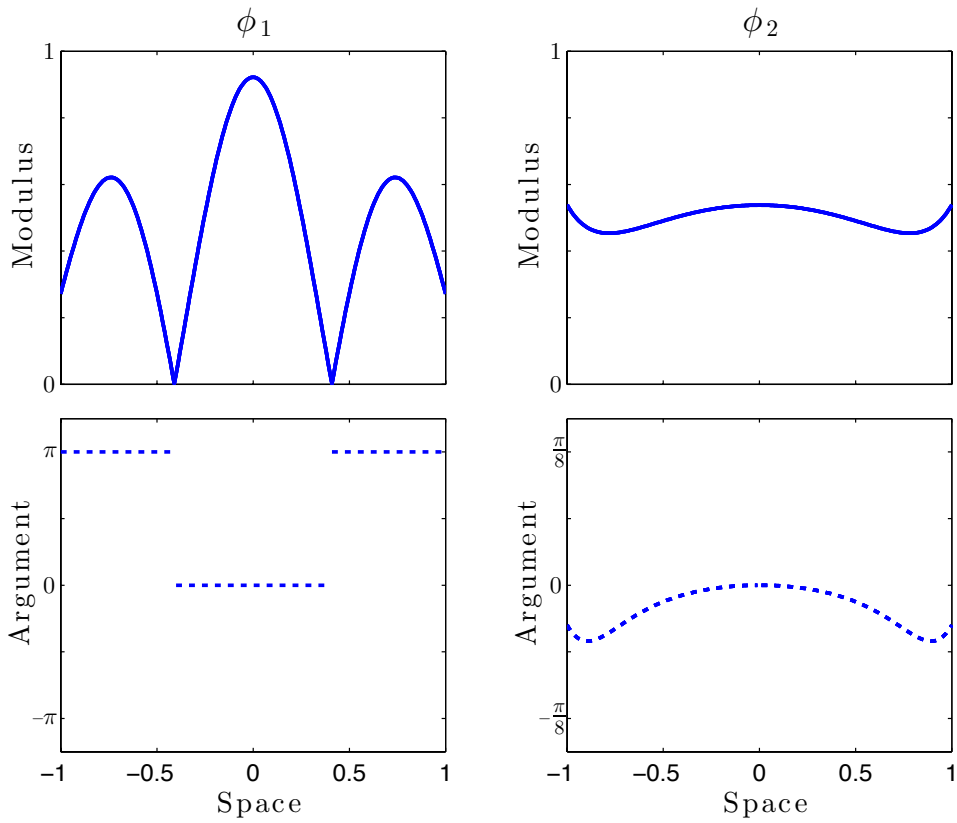


FIGURE 5.1: Modulus and argument of eigenfunctions ϕ corresponding to critical eigenvalues $\lambda = 0$ on the *left* and $\lambda = 0.7062i$ on the *right*.

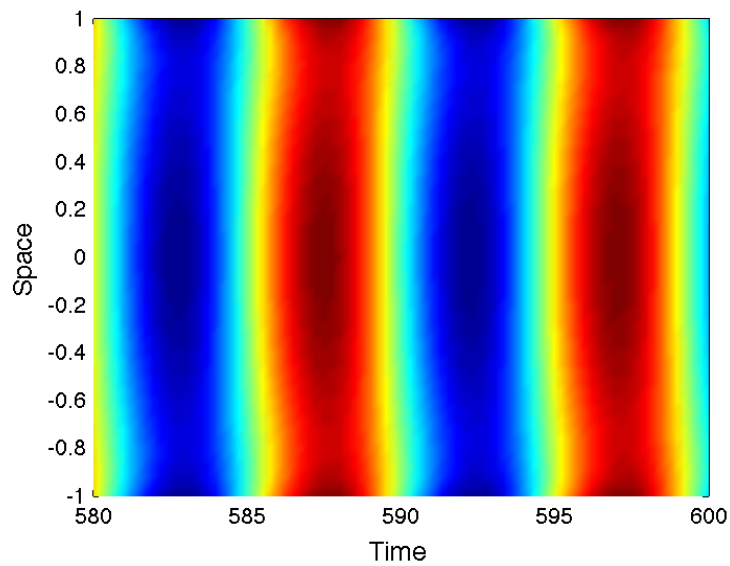


FIGURE 5.2: Close-up of figure 4.1, *bottom*.

Part II.

Relation to spiking neuron models

6. A spiking neuron network

6.1. Spiking neuron model

In the Rulkov model [18, 19], neurons are point-like elements with two state variables, the membrane potential v and a recovery variable r with no direct biological resemblance (Rulkov denotes these variables with x and y respectively). The model is purely phenomenological but can replicate all kinds of spiking behaviour of real biological neurons and since it is discrete in time, it has high computational efficiency.

In this thesis we use a modified version of the Rulkov map. In our case the dependence of the recovery variable on the membrane potential is implicit instead of explicit, making the map harder to analyse but better suitable for a mean field approximation. The modified model is given by the following map

$$v_{n+1} = f_\alpha(v_n, v_{n-1}, \sigma + r_n + \beta I_n) \quad (6.1a)$$

$$r_{n+1} = r_n + \mu(-r_n + (1 - \beta)I_n - \rho s_n) \quad (6.1b)$$

with f_α a piecewise continuous function defined as

$$f_\alpha(v_n, v_{n-1}, y) = \begin{cases} \frac{\alpha}{1 - v_n} + y & \text{if } v_n \leq 0 \\ \alpha + y & \text{if } 0 < v_n < \alpha + y \text{ and } v_{n-1} \leq 0 \\ -1 & \text{otherwise} \end{cases} \quad (6.2)$$

Figure 6.1 shows an illustration of this function.

The parameter σ determines the activity in the absence of any input (which is equivalent to constant input by a change of variables) and ρ sets the influence of a single spike on the recovery variable r with time scale parameter $\mu < 1$. External input (e.g. synaptic currents) is modelled through variable I_n and the parameter β determines how this input is applied to the map. The dependence of (6.1b) on v_n is due to the indicator variable s_n defined by

$$s_n = \begin{cases} 1 & \text{if the neuron spiked at iteration } n \\ 0 & \text{otherwise} \end{cases} \quad (6.3)$$

From (6.2) follows that the spiking condition in (6.3) is satisfied when

$$(v_n \geq \alpha + \sigma + r_n + \beta I_n > 0) \quad \vee \quad (v_n > 0 \wedge v_{n-1} > 0) \quad (6.4)$$

The dependence of f_α on v_{n-1} forces the map to always iterate its trajectory from the middle interval to the rightmost one. This assures that the duration of a spike is always exactly one iteration. Without this dependence, the map could stay in the middle interval for several iterations if the input is monotonically increasing. After one iteration at the middle interval and one iteration at the right interval the map stays at least one iteration in the left interval. Therefore, the maximal firing rate of a neuron is once in three iterations.

Fixed points and periodic trajectories

A neuron is quiescent if its membrane potential is at (or converges to) a fixed point whereas spiking corresponds to a periodic trajectory.

For constant input the dependence of f_α on v_{n-1} can be ignored. If we assume for the moment that r_n is constant we can analyse the one-dimensional map $v_{n+1} = f_\alpha(v_n, y)$. An example is shown in figure 6.1. For $y < 1 - 2\sqrt{\alpha}$ there exists a stable fixed point v_s and an unstable fixed point v_u given by

$$v_s = \frac{y+1}{2} - \frac{1}{2}\sqrt{(y-1)^2 - 4\alpha} \quad (6.5a)$$

$$v_u = \frac{y+1}{2} + \frac{1}{2}\sqrt{(y-1)^2 - 4\alpha} \quad (6.5b)$$

At $y = 1 - 2\sqrt{\alpha}$ the two fixed points coincide at a saddle-node bifurcation and disappear for $y > 1 - 2\sqrt{\alpha}$.

A periodic trajectory exists if there are no fixed points or if the unstable fixed point (6.5b) lies to the left of -1 (see figure 6.1). Since the point $v = -1$ is part of every periodic trajectory, there can't exist more than one periodic orbit for every value of y . A stable fixed point and a periodic orbit can only coexist for $\alpha > 4$. The map $v_{n+1} = f_\alpha(v_n, y)$ then is bistable for

$$y \in \left(-\left(1 + \frac{\alpha}{2}\right), 1 - 2\sqrt{\alpha} \right) \quad (6.6)$$

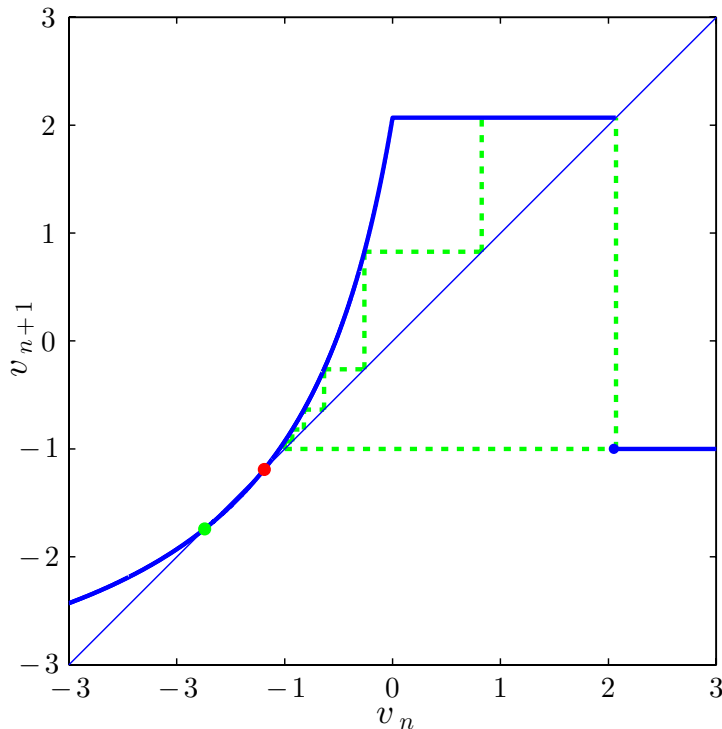


FIGURE 6.1: Illustration of $f_\alpha(v_n, y)$ (thick blue line) for $\alpha = 6$ and $y = -3.93$ with stable fixed point (green dot), unstable fixed point (red dot) and stable periodic trajectory (dashed green line).

Spiking dynamics

It follows that for $\alpha \leq 4$ and no input a neuron is quiescent for $\sigma \leq 1 - 2\sqrt{\alpha}$ and spiking for $\sigma > 1 - 2\sqrt{\alpha}$. We now show how a few typical types of spiking dynamics of real biological neurons can be replicated with the modified Rulkov model (6.1).

- *Fast spiking* cells are characterized by the fact that they fire spike trains with practically no spike-frequency adaptation. This can be achieved by choosing a rather large value for μ . In this case the influence of a single spike on the recovery variable r decays very fast, therefore the value of r_n is dominated by the timing of the last spike and the influence of older spikes can be neglected (see figure 6.2A). Since the time scales of (6.1a) and (6.1b) are similar the value of β has no influence on the qualitative dynamics in this case. Because of the lack of adaptation, the spiking rate of a fast spiking neuron can be very well approximated by a function of the current input I .
- *Spike-frequency adaptation* can be modeled with $\mu \ll 1$. The recovery variable then acts as a slow time scale, so it takes a while until r_n fully responds to a change in input. The level of adaptation can be controlled with β . An example is shown in figure 6.2B.
- *Bursting* is only possible if (6.1a) can be bistable, which is the case for $\alpha > 4$. This is illustrated by the example in figure 6.2C. A burst is initiated when the slow variable r_n reaches its maximal value. At that point the stable fixed point has disappeared so the cell starts spiking. This spiking leads to a decrease of r_n which slows down the spiking frequency. When r_n has reached its minimum, the unstable fixed point has moved through -1 which terminates the periodic orbit and therefore the spiking. The membrane potential v_n now converges to the stable fixed point and since the spiking has stopped, the slow variable starts increasing again. A new periodic orbit appears, but because its membrane potential is close to the stable fixed point the cell doesn't start spiking until the fixed point disappears and a new burst is initiated. The model can mimic tonic bursting (chattering) as well as intrinsic bursting (figure 6.2D).
- *Rebound spikes/bursts* are induced by a hyperpolarizing current which is suddenly switched off. Through this mechanism, action potentials can be triggered by inhibitory input. In the model this is only possible for $\beta > 1$. In that case the recovery variable builds up while the cell gets hyperpolarized. Examples are shown in figure 6.3E and figure 6.3F.

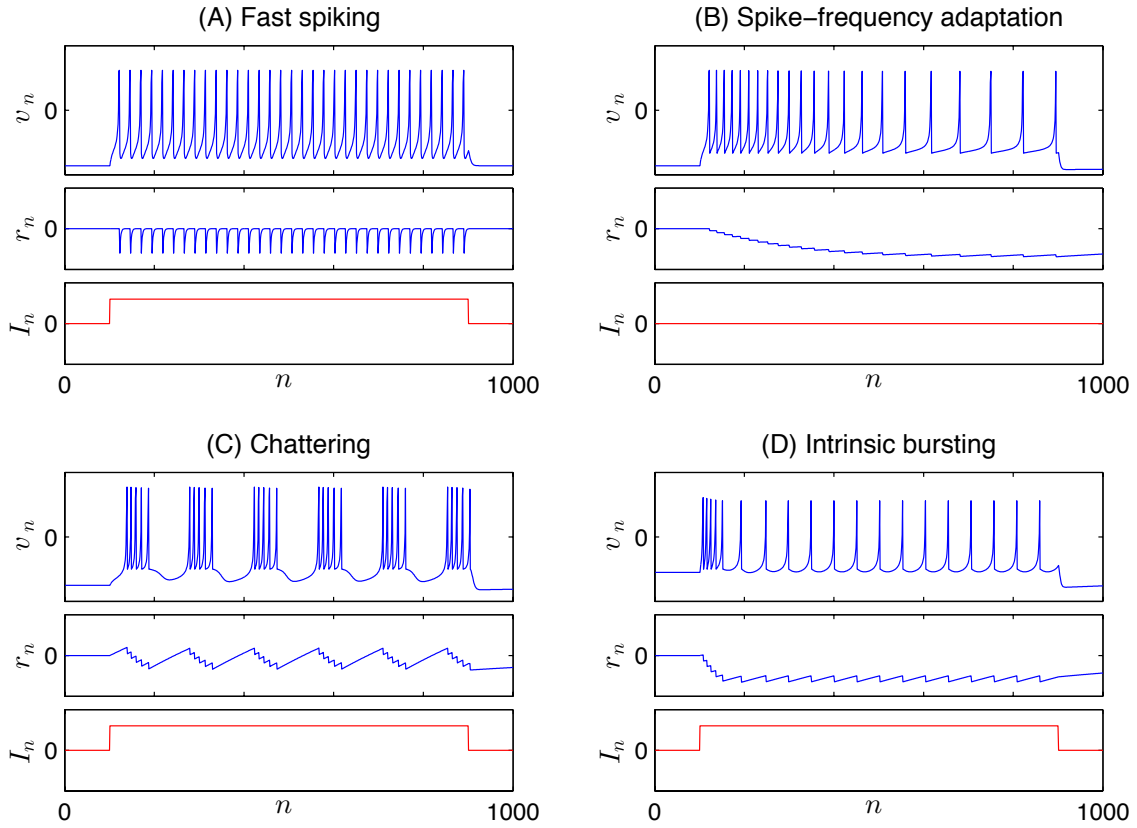


FIGURE 6.2: Response of quiescent neurons to excitatory input. Parameter values $(\alpha, \sigma, \beta, \mu, \rho)$ given by *A*: $(3.8, -2.95, 1, 0.4, 0.3)$; *B*: $(3.8, -2.95, 1, 0.001, 2)$; *C*: $(5, -3.5, 0.1, 0.002, 8)$; *D*: $(4.2, -3.1, 0.4, 0.002, 15)$;

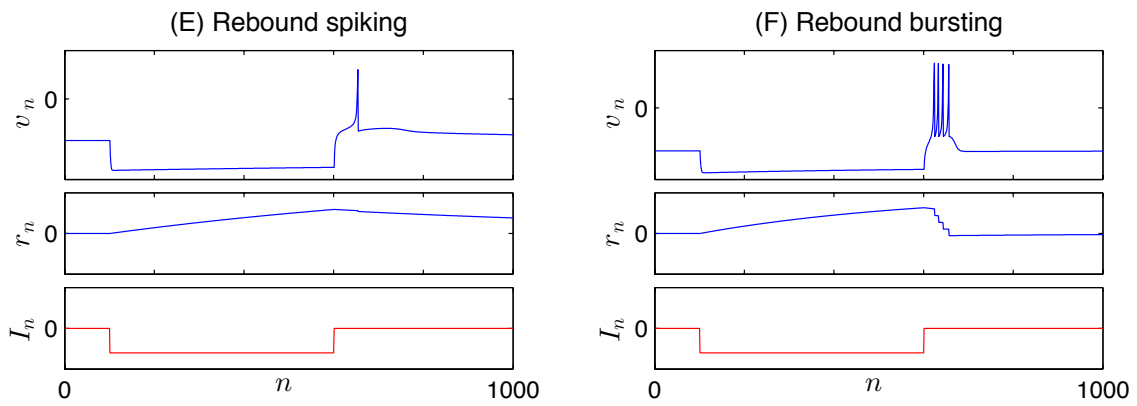


FIGURE 6.3: Response of quiescent neurons to inhibitory input. Parameter values $(\alpha, \sigma, \beta, \mu, \rho)$ given by *E*: $(3.8, -2.95, 1.5, 0.001, 2)$; *F*: $(5, -3.5, 1.5, 0.002, 8)$

6.2. Synaptic currents

At a synapse, the arrival of a presynaptic action potential results into the release of neurotransmitter, which in turn cause ion channels on the postsynaptic side to open. This

leads to a conductance change of the postsynaptic membrane and therefore induces an ohmic current. For simplicity we assume that a neurons spends most of its time close to rest, so that we can approximate the membrane potential by a constant and effectively model the arrival of a spike as generating a synaptic current rather than a conductance change [4].

Since our neurons are modeled as point-like elements all internal properties such as the dendritic tree are ignored. We assume that postsynaptic currents decay exponentially and that the decay is dominated by the postsynaptic membrane, which is the case if the synapses are fast. Under these assumptions, the shape of an isolated postsynaptic current only depends on the postsynaptic neuron.

In a network consisting of N neurons let τ_{ij} denote the time it takes for a presynaptic spike of neuron j to reach the postsynaptic neuron i . Assuming that the synaptic responses sum linearly, the total synaptic current $u_n^{(i)}$ to neuron i is given by the difference equation

$$u_{n+1}^{(i)} = \gamma_i u_n^{(i)} + \sum_{j=1}^N w_{ij} s_{n+1-\tau_{ij}}^{(j)} \quad (6.7)$$

with $0 < \gamma_i < 1$ given by the membrane time constant of neuron i , w_{ij} the connection weight from neuron j to neuron i and $s_n^{(i)}$ as defined in (6.3) and (6.4). Note that the delays τ_{ij} are given in iterations of the map, so they are non-negative integers.

Remark Under the above assumptions, the total synaptic current $u_i(t)$ to neuron i is, in continuous time, given by

$$u_i(t) = \sum_{j=1}^N \sum_m w_{ij} e^{-\nu_i(t-T_j^m-\tau_{ij})} \Theta(t - T_j^m - \tau_{ij}) \quad (6.8)$$

with $\{T_j^m, m \in \mathbb{Z}\}$ the spiking times of neuron j , $\Theta(x)$ the Heaviside step function and time scaled such that one unit of time corresponds to one iteration of the Rulkov map.

Using

$$\Theta(x+1) = \Theta(x) + \varphi(x) \quad \text{with} \quad \varphi(x) = \begin{cases} 1 & \text{if } x \in [-1, 0) \\ 0 & \text{else} \end{cases} \quad (6.9)$$

equation (6.8) can be rewritten as

$$u_i(t+1) = e^{-\nu_i} u_i(t) + \sum_{j=1}^N \sum_m w_{ij} e^{-\nu_i(t+1-T_j^m-\tau_{ij})} \varphi(t - T_j^m - \tau_{ij}) \quad (6.10)$$

The second sum in (6.10) is only nonzero if $\exists T \in \{T_j^m, m \in \mathbb{Z}\}$ with

$$t - \tau_{ij} < T \leq t + 1 - \tau_{ij} \quad (6.11)$$

Since in our network the spiking times T_j^m and delays τ_{ij} are integers equation (6.10) reduces to (6.7).

6.3. Connectivity

Using notation as in [3], we consider a multilayer network consisting of M different populations. Suppose the neurons are labeled by $i \in P_k$, $k = 1, \dots, M$ and $|P_k| = N_k$. Each population is placed on the one-, two- or three-dimensional spatial domain Ω .

We assume that the connection probability p_{ij} and delay τ_{ij} between neuron $i \in P_k$ and neuron $j \in P_l$ only depends on k and l and their distance d_{ij} and have the form

$$p_{ij} = e^{-b_{kl}d_{ij}} \quad (6.12)$$

$$\tau_{ij} = a_{kl} + \frac{d_{ij}}{c_{kl}} \quad (6.13)$$

with conduction speeds c_{kl} and 'intrinsic' delays a_{kl} . Since the delays are given in iterations of the map, all arising delays τ_{ij} are rounded to the nearest integer.

If a connection exists, the connection weight w_{ij} only depends on k and l and is normalized by the maximal number of incoming connections of the same type.

$$w_{ij} = \frac{W_{kl}}{N_l} \quad (6.14)$$

Within one population all neurons share the parameters α, β, μ, ρ and γ . To assure that the neurons spike asynchronously the values of σ are drawn from some random distribution. This basically means that the neurons in the network receive random (but constant) 'background input'. Why the assumption of asynchronous spiking is essential in the mean field reduction is explained in section 7.

7. From network to mean field

The reduction from a spiking neuron network to a single mean field equation is done in two steps. In the first step the connection between the neurons in the network are averaged, leading to a new network with deterministic all-to-all connectivity. The second step is the crucial step: a short-time temporal averaging converts individual spikes to spiking rates. In this step all information contained in the exact timing of spikes is lost. This so-called 'problem of neural coding' is a subject of ongoing debate [10]. It is here where the assumption of asynchronous spiking becomes necessary, because the conversion to rates 'destroys' correlations in spike timing.

7.1. Averaging connectivity

Let us again look at two neurons $i \in P_k$ and $j \in P_l$. For large N_k , $k = 1, \dots, M$ we can approximate the connectivity by an all-to-all connectivity with 'expected weights' \bar{w}_{ij} given by

$$\bar{w}_{ij} = w_{ij} p_{ij} = e^{-b_{kl} d_{ij}} \frac{W_{kl}}{N_l} \quad (7.1)$$

To make things concrete, let's consider a two-layer network consisting of an excitatory (E) and an inhibitory (I) population, both equidistantly placed on the one-dimensional spatial domain $\Omega = [-1, 1]$. We take $N_E = N_I = N$, so the distance between adjacent cells of the same type is given by $h = \frac{2}{N-1}$. Assuming that delays only depend on distance the synaptic currents (6.7) can be written as

$$u_{n+1}^{(E,i)} = \gamma_E u_n^{(E,i)} + \frac{1}{N} \sum_{j=1}^N w_{EE}(|i-j|h) s_{n-\tau(|i-j|h)}^{(E,j)} - w_{EI}(|i-j|h) s_{n-\tau(|i-j|h)}^{(I,j)} \quad (7.2a)$$

$$u_{n+1}^{(I,i)} = \gamma_I u_n^{(I,i)} + \frac{1}{N} \sum_{j=1}^N w_{IE}(|i-j|h) s_{n-\tau(|i-j|h)}^{(E,j)} - w_{II}(|i-j|h) s_{n-\tau(|i-j|h)}^{(I,j)} \quad (7.2b)$$

with connectivity functions

$$w_{XY}(d) = W_{XY} e^{-b_{XY} d} \quad \text{with } X, Y \in \{E, I\} \quad (7.3)$$

and delays

$$\tau(d) = a + \frac{d}{c} \quad (7.4)$$

If we choose $\gamma_E = \gamma_I = \gamma$ and assume that the connection functions are independent of the postsynaptic neuron type, that is

$$w_{EE}(d) = w_{IE}(d) = w_E(d) \quad (7.5a)$$

$$w_{EI}(d) = w_{II}(d) = w_I(d) \quad (7.5b)$$

we can take $u_n^{(E,i)} = u_n^{(I,i)}$ and (7.2) reduces to

$$u_{n+1}^{(i)} = \gamma u_n^{(i)} + \frac{1}{N} \sum_{j=1}^N w_E(|i-j|h) s_{n-\tau(|i-j|h)}^{(E,j)} - w_I(|i-j|h) s_{n-\tau(|i-j|h)}^{(I,j)} \quad (7.6)$$

To make a last simplification, we make the artificial assumption that neurons from the two populations are pairwise identical, that is $\alpha_E = \alpha_I$, $\beta_E = \beta_I$, $\mu_E = \mu_I$, $\rho_E = \rho_I$ and $\sigma_{E,i} = \sigma_{I,i}$ for all $i = 1, \dots, N$. Since both populations receive the same synaptic input and their 'inner properties' are identical there holds $s_n^{(E,i)} = s_n^{(I,i)}$ for all n, i and the synaptic current is given by

$$u_{n+1}^{(i)} = \gamma u_n^{(i)} + \frac{1}{N} \sum_{j=1}^N w(|i-j|h) s_{n-\tau(|i-j|h)}^{(j)} \quad (7.7)$$

with

$$w(d) = w_E(d) - w_I(d) = W_E e^{-b_E d} - W_I e^{-b_I d} \quad (7.8)$$

Equation (7.7) effectively models a mixed population of excitatory and inhibitory neurons with similar dynamical properties.

7.2. From spikes to rates

Until now, all expressions for the synaptic currents were event based, since synaptic currents are induced by spikes of neurons. If we average these equations over some short time interval, we can approximate the 'spiking variable' $s_n \in \{0, 1\}$ by the spiking rate F .

As we saw before, for $\alpha \leq 4$ (no bursting) and μ rather large, spike-frequency adaptation can be neglected (see figure 6.2A). For fixed α , μ , ρ and constant input I the spiking rate F of a neuron then is a (piecewise constant) function of $\sigma + I$ and can easily be determined numerically.

In our network the values of σ are drawn from a random distribution with some probability density function g . The 'expected firing rate' \bar{F} of a neuron in the network is then given by

$$\bar{F}(I) = \int_{-\infty}^{\infty} g(s) F(s + I) ds \quad (7.9)$$

Example We choose $\alpha = 3.8$, $\mu = 0.4$, $\rho = 0.25$ and let σ be a random variable given by

$$\sigma = 1 - 2\sqrt{\alpha} + Z \quad (7.10)$$

with $Z \sim N(0, 1)$. The rate functions F and \bar{F} are computed numerically and shown in figure 7.1. The 'expected firing rate' \bar{F} can be very well approximated by a function of the form

$$S(x) = \frac{S_{\max}}{1 + e^{-\kappa(x-\theta)}} \quad (7.11)$$

which is also illustrated in figure 7.1.

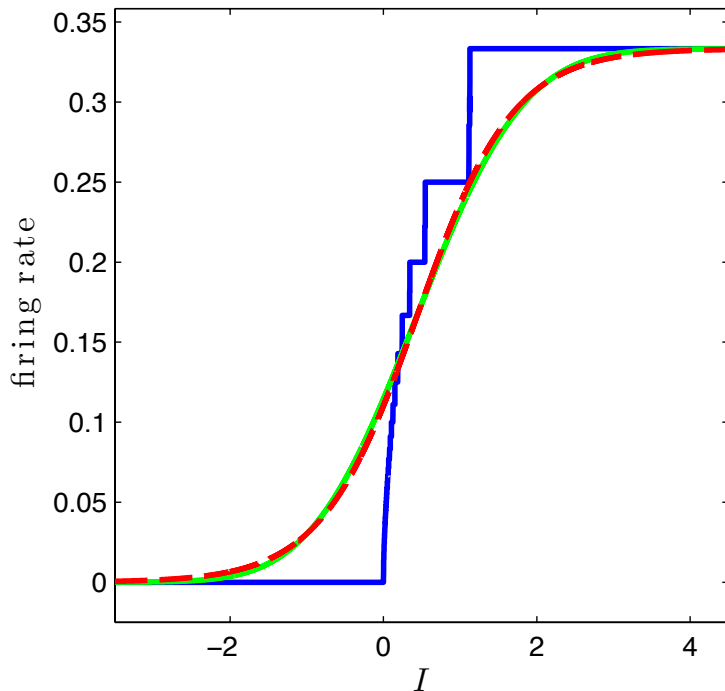


FIGURE 7.1: Illustration of $F(1 - 2\sqrt{\alpha} + I)$ for $\alpha = 3.8$, $\mu = 0.4$ and $\rho = 0.25$ (blue line), $\bar{F}(I)$ for σ as given in (7.10) (green line) and $S(I)$ with $S_{\max} = \frac{1}{3}$, $\kappa = 1.6$ and $\theta = 0.44$ (dashed red line).

Substituting the approximated expected firing rate S for s in equation (7.7) leads to

$$u_{n+1}^{(i)} = \gamma u_n^{(i)} + \frac{1}{N} \sum_{j=1}^N w(|i-j|h) S(u_{n-\tau(|i-j|h)}^{(j)}) \quad (7.12)$$

We have here assumed that the synaptic currents u_i are slowly varying compared to the spiking dynamics. By interpreting the sum in (7.12) as a Riemann sum we rewrite (7.12) as

$$u_{n+1}(ih) = \gamma u_n(ih) + \frac{N-1}{2N} \sum_{j=1}^N hw(|i-j|h) S(u_{n-\tau(|i-j|h)}(jh)) \quad (7.13)$$

which for $N \rightarrow \infty$ converges to

$$u_{n+1}(x) = \gamma u_n(x) + \frac{1}{2} \int_{-1}^1 w(|x-y|) S(u_{n-\tau(|x-y|)}(y)) dy \quad (7.14)$$

This in turn can be seen as the forward Euler of

$$\frac{\partial}{\partial t} u(x, t) = -\vartheta u(x, t) + \frac{1}{2} \int_{-1}^1 w(|x-y|) S(u(y, t - \tau(|x-y|))) dy \quad (7.15)$$

with $\vartheta = 1 - \gamma$.

We conclude this section with three examples of different spatial-temporal patterns generated by two-layer neuron networks with random connections, their averaged single-layer counterparts (7.7) and the mean field reduction (7.15).

In all examples we fix the (neuron) parameters $\alpha = 3.8$, $\beta = 1$, $\mu = 0.4$, $\rho = 0.25$ and $\gamma = 0.9$. The values of σ are given by

$$\sigma = 1 - 2\sqrt{\alpha} + \frac{1}{2}Z \tag{7.16}$$

where Z is drawn from $N(0, 1)$.

For the firing rate in mean field we use equation (7.11) with $S_{\max} = \frac{1}{3}$, $\kappa = 1.8$ and $\theta = 0.37$. The connectivity and delay functions are varied.

7.3. Example 1: A stationary 2-bump

Figure (7.2) shows the result of simulations with the 'wizard hat' connectivity and delay function given by

$$w(d) = 20e^{-5d} - 10e^{-2d} \quad (7.17)$$

$$\tau(d) = 40 + 10d \quad (7.18)$$

We observe a stationary solution with two active bumps at the borders of the domain which is very well reproduced by the mean field solution.

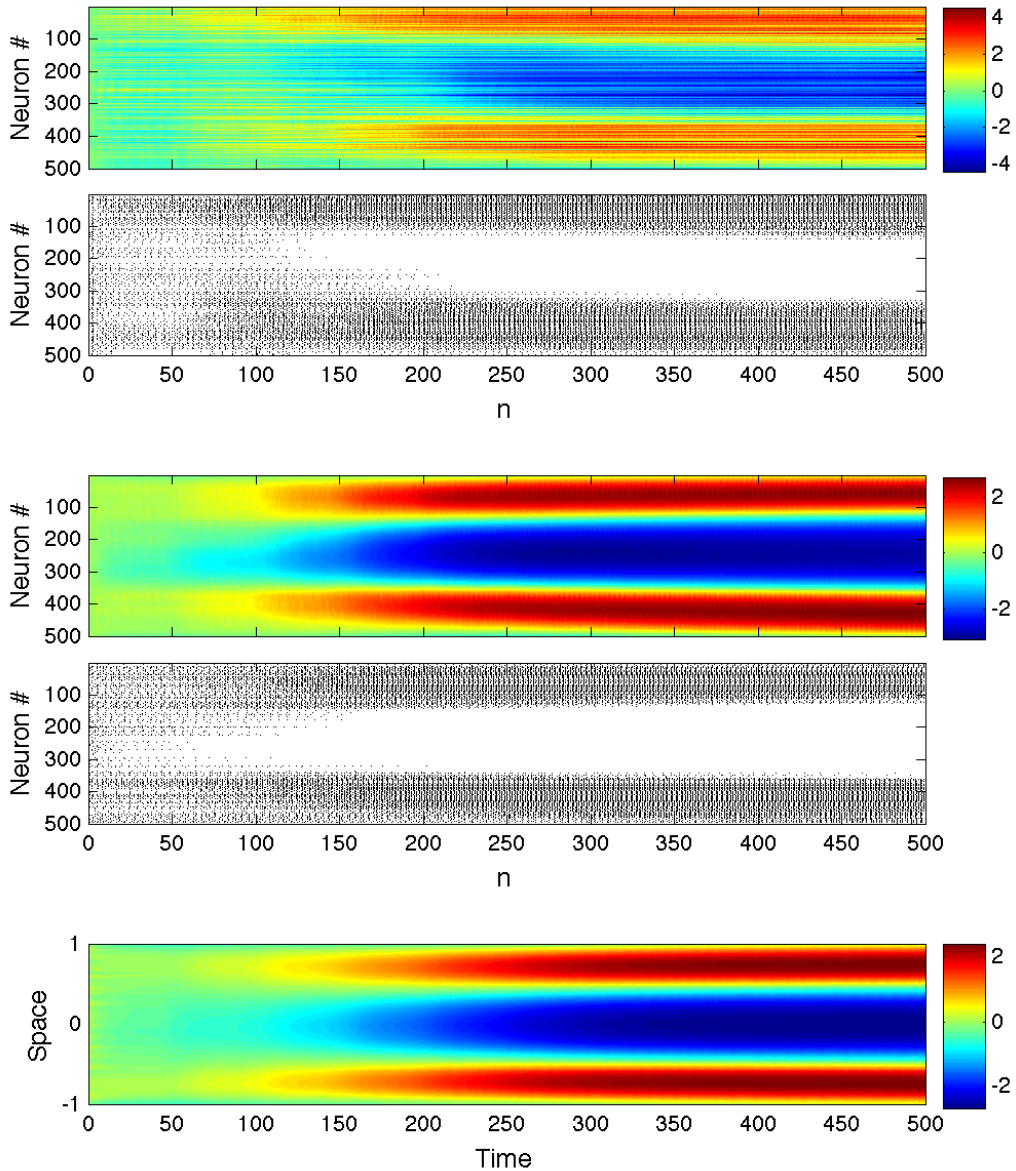


FIGURE 7.2: *Top*: One run of a network with random connections (only excitatory population). *Middle*: One run of the mixed network with averaged connectivity (7.7). *Bottom*: Solution of mean field equation (7.15).

7.4. Example 2: A travelling wave

In this example we use the same delay (7.18) but invert the connectivity.

$$w(d) = 10e^{-2d} - 20e^{-5d} \quad (7.19)$$

This 'inverted wizard hat' connectivity leads to a travelling wave as is shown in figure 7.3. Again the agreement with the mean field reduction is very good.

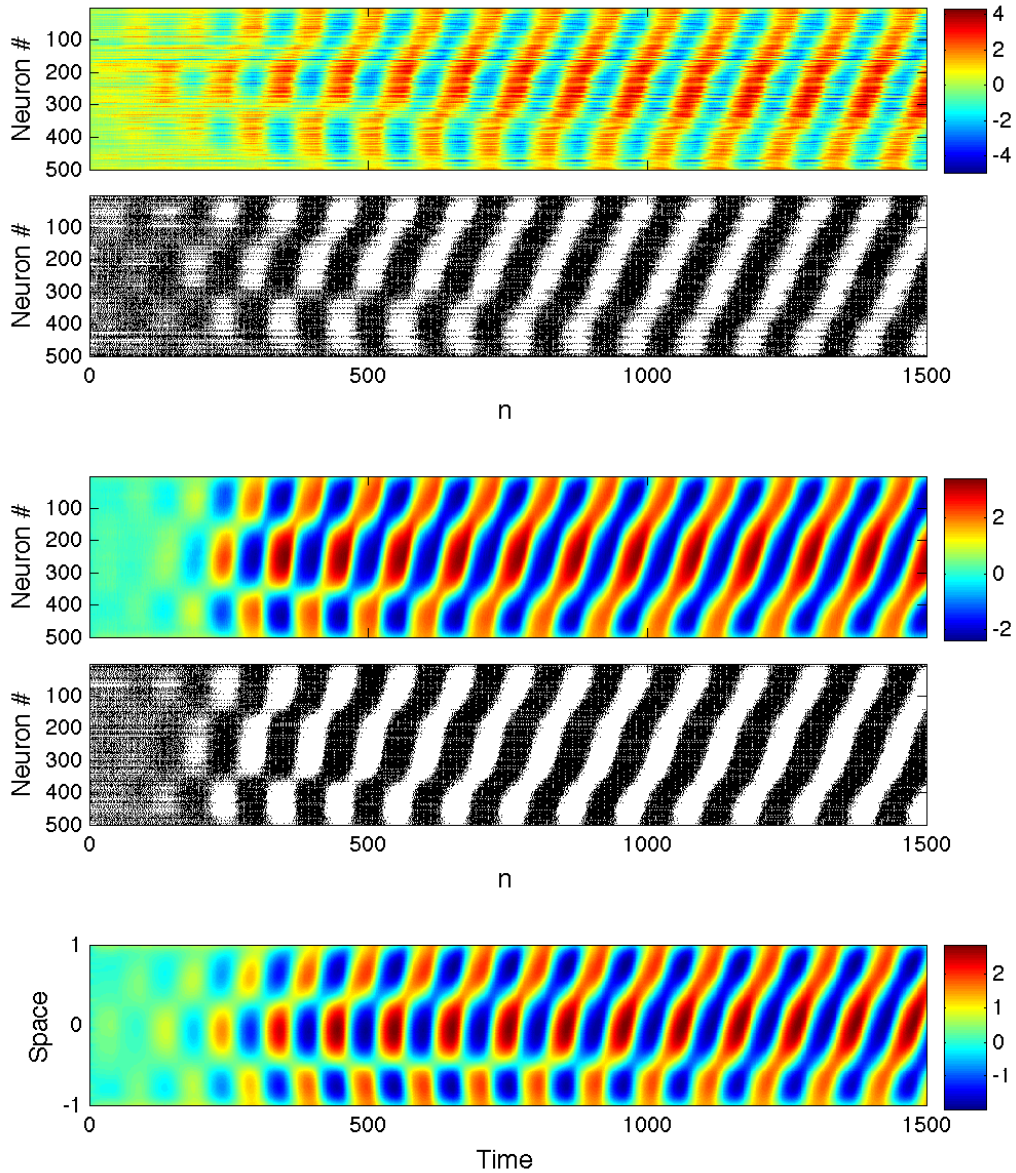


FIGURE 7.3: *Top*: One run of a network with random connections (only excitatory population). *Middle*: One run of the mixed network with averaged connectivity (7.7). *Bottom*: Solution of mean field equation (7.15).

7.5. Example 3: A standing wave

The traveling waves of example 2 turn into standing waves if we slow down the conduction speed.

$$\tau(d) = 40 + 50d \tag{7.20}$$

Figure 8.1 again shows a very good agreement of the mean field reduction.

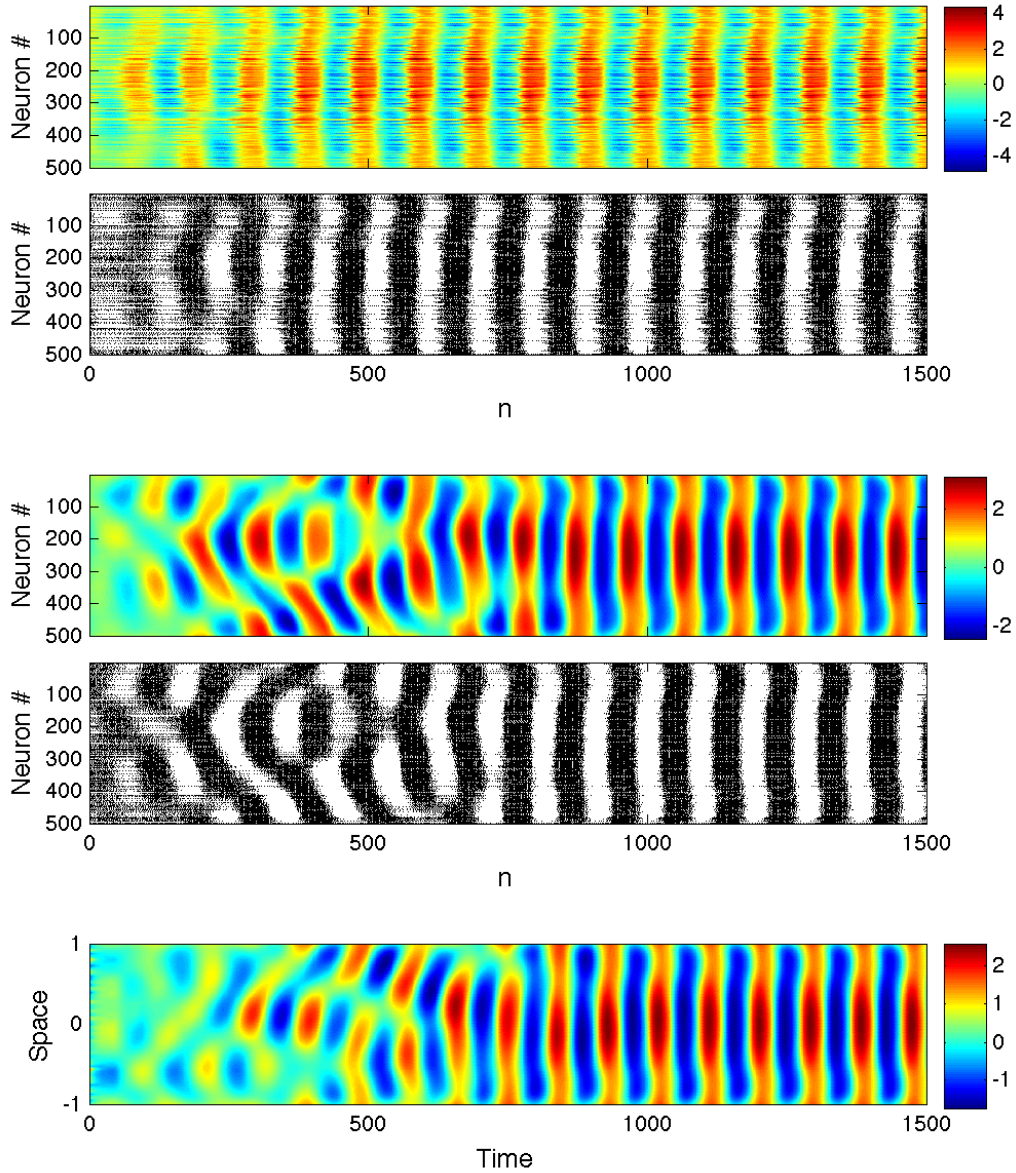


FIGURE 7.4: *Top:* One run of a network with random connections (only excitatory population). *Middle:* One run of the mixed network with averaged connectivity (7.7). *Bottom:* Solution of mean field equation (7.15).

8. Adding spike-frequency adaptation

In section 7 we restricted to cells without spike-frequency adaptation. It is now straightforward to implement more general cases where the recovery variable r can be slow.

We again assume that bursting is not possible ($\alpha \leq 4$). As we showed in section 6 the map (6.2) then has a periodic trajectory if and only if

$$y > 1 - 2\sqrt{\alpha} \quad (8.1)$$

From (6.1) follows that the spiking rate of a Rulkov neuron is a function of $\sigma + r + \beta I$. For every value of $y = \sigma + r + \beta I$ satisfying (8.1) we can compute the period of limit cycle which gives us the spiking rate of the neuron. For other values of y the spiking rate is zero.

In the same way as in section 7 we can approximate the expected firing rate $S(r + I)$ and substitute this function for s_n in (6.1b) and (7.7). The mean field approximation of the Rulkov network with spike-frequency adaptation is then given by

$$\frac{\partial}{\partial t} u(x, t) = -\vartheta u(x, t) + \frac{1}{2} \int_{-1}^1 w(|x - y|) S\left(r(y, t - \tau(|x - y|)) + \beta u(y, t - \tau(|x - y|))\right) dy \quad (8.2a)$$

$$\frac{\partial}{\partial t} r(x, t) = \mu \left[(1 - \beta)u(x, t) - r(x, t) - \rho S(r(x, t) + \beta u(x, t)) \right] \quad (8.2b)$$

8.1. Example 4: A moving bump

We conclude with a last example illustrating equation (8.2). Parameter values of the recovery variable are given by $\mu = 0.001$ and $\rho = 20$ respectively. The connectivity is chosen as

$$w(d) = 30e^{-5d} - 15e^{-2d} \quad (8.3)$$

and other parameters are the same as in example 1 in section 7. Neurons with these parameters show a high level of spike-frequency adaptation. Figure 7.4 shows a simulation of the network and the corresponding solution of (8.2). We observe that spike-frequency adaptation leads to a 'moving bump' solution. This can be explained as follows: At a bump of activity the value of r slowly decreases. Since this suppresses the activity the bump starts to wander to regions where r is higher. The timescale at which this happens is set by the recovery variable and therefore the period is much larger than in the oscillations previously observed in examples 2 and 3.

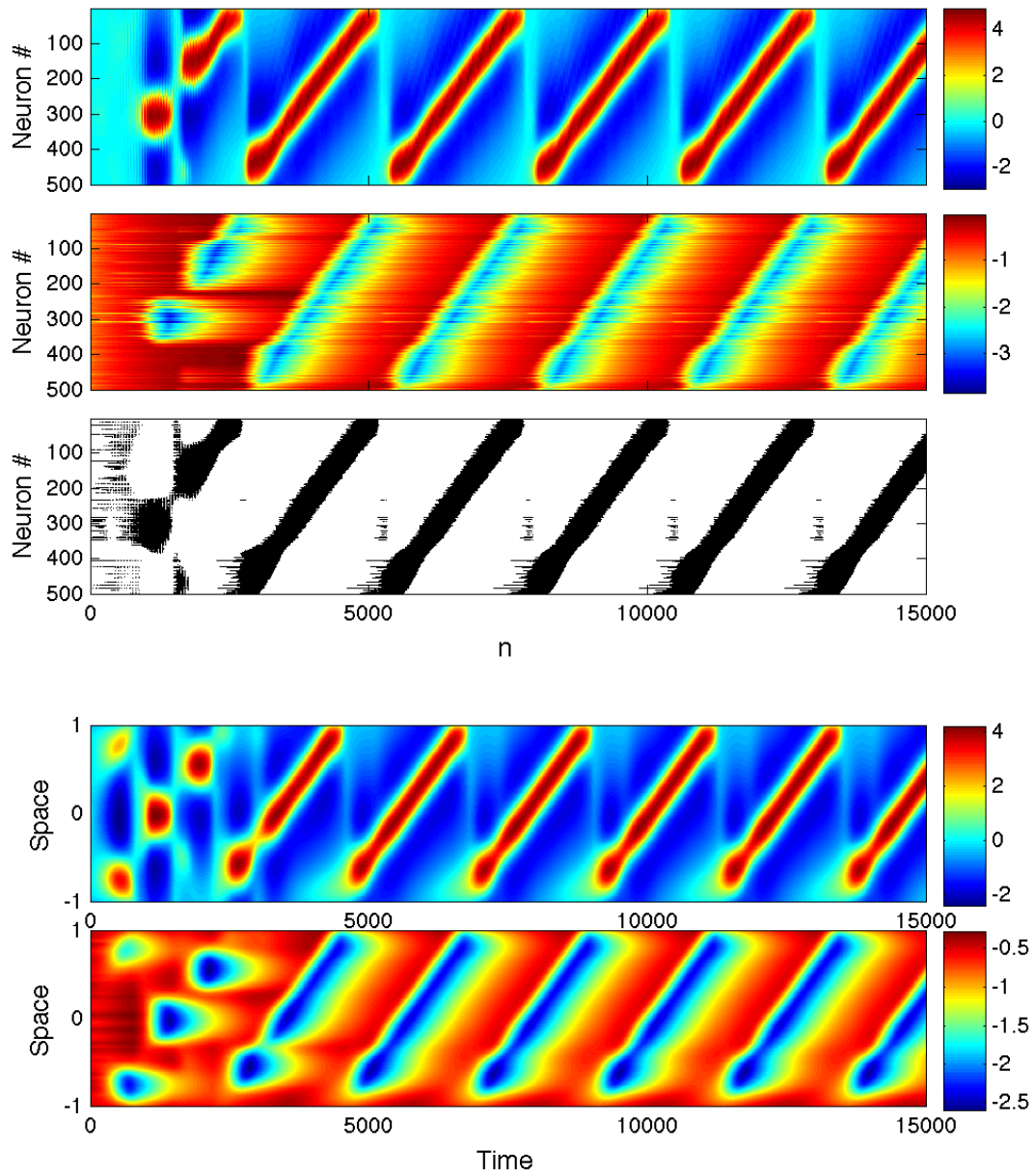


FIGURE 8.1: *Top:* One run of the mixed network with averaged connectivity (7.7).
Bottom: Solution of the modified mean field equation (8.2).
 The first plots shows the synaptic currents, the second plots the recovery variables r .

9. Discussion

In the second part of this thesis we have demonstrated how a particular spiking neuron network can be reduced to a mean field equation. This opens the door for numerical and analytical studies which would not have been possible for the original spiking neuron network. An example of such a study is given in the first part of this thesis.

Simulations show that the agreement of the mean field reduction with the spiking neuron network is very good, while the parameter correspondence is clear.

The crucial step in the reduction is the translation from individual spikes to spiking rates, and it is here where problems arise. While the spiking neuron model can replicate a wide variety of biologically realistic spiking patterns, the reduction is only valid for non-bursting neurons, which drastically reduces the cases in which the reduction can be used.

Another problem is the way the firing rate function is approximated. This is done 'by hand', which is ambiguous and therefore not very scientific.

We conclude with an issue indicated in section 7, the 'problem of neural coding'. Obviously, all information contained in the exact timing of individual spikes is lost when making the transition to rate models. Whether or not this information is essential to describe brain activity is still a topic of ongoing debate, but more than that, this gives another restriction on our spiking neuron network: we have to assume that spike timings are uncorrelated. Reductions of networks violating this last assumption may however still capture useful information. This would be an interesting topic for further research.

References

- [1] S. Amari, *Homogeneous nets of neuron-like elements*, Biol. Cybernet. **17** (1975), no. 4, 211–220.
- [2] ———, *Dynamics of pattern formation in lateral-inhibition type neural fields*, Biol. Cybernet. **27** (1977), no. 2, 77–87.
- [3] P. C. Bressloff, *Stochastic neural field theory and the system-size expansion*, SIAM J. Appl. Math **70** (2009), no. 5, 1488–1521.
- [4] ———, *Spatiotemporal dynamics of continuum neural fields*, J. Phys. A **45** (2012), no. 3, 033001, 109.
- [5] S. A. Campbell, *Time delays in neural systems*, Handbook of Brain Connectivity, Springer, Berlin, 2007, pp. 65–90.
- [6] S. Coombes and C. Laing, *Delays in activity-based neural networks*, Philos. Trans. R. Soc. Lond. Ser. A Math. Phys. Eng. Sci. **367** (2009), no. 1891, 1117–1129.
- [7] R. Curtu and B. Ermentrout, *Pattern formation in a network of excitatory and inhibitory cells with adaptation*, SIAM J. Appl. Dyn. Syst. **3** (2004), no. 3, 191–231.
- [8] K. Engelborghs, T. Luzyanina, and D. Roose, *Numerical bifurcation analysis of delay differential equations using DDE-BIFTOOL*, ACM Trans. Math. Software **28** (2002), 1–21.
- [9] G. Faye and O. Faugeras, *Some theoretical and numerical results for delayed neural field equations*, Phys. D **239** (2010), no. 9, 561–578.
- [10] W. Gerstner and W. M. Kistler, *Spiking neuron models*, Cambridge University Press, Cambridge, 2002, Single neurons, populations, plasticity.
- [11] J. Guckenheimer and P. Holmes, *Nonlinear oscillations, dynamical systems, and bifurcations of vector fields*, Applied Mathematical Sciences, vol. 42, Springer, New York, 1983.
- [12] A. Hutt and F. M. Atay, *Effects of distributed transmission speeds on propagating activity in neural populations*, Phys. Rev. E (3) **73** (2006), no. 2, 021906, 5.
- [13] E. M. Izhikevich, *Simple model of spiking neurons*, IEEE Trans. Neural Networks **14** (2003), 1569–1572.
- [14] Z. P. Kilpatrick and P. C. Bressloff, *Effects of synaptic depression and adaptation on spatiotemporal dynamics of an excitatory neuronal network*, Phys. D **239** (2010), no. 9, 547–560.

-
- [15] Yu. A. Kuznetsov, *Elements of applied bifurcation theory*, 3rd ed., Applied Mathematical Sciences, vol. 112, Springer, New York, 1998.
- [16] P. L. Nunez, *The brain wave equation: A model for the EEG*, Math. Biosci. **21** (1974), no. 3-4, 279–297.
- [17] A. Roxin and E. Montbrió, *How effective delays shape oscillatory dynamics in neuronal networks*, Phys. D **240** (2011), no. 3, 323–345.
- [18] N. F. Rulkov, *Modeling of spiking-bursting neural behavior using two-dimensional map*, Phys. Rev. E **65** (2002), 041922.
- [19] N. F. Rulkov, I. Timofeev, and M. Bazhenov, *Oscillations in large-scale cortical networks: Map-based model*, J. Comput. Neurosci. **17** (2004), 203–223.
- [20] W. van Drongelen, H. C. Lee, M. Hereld, D. Jones, M. Cohoon, F. Elsen, M. E. Papka, and R. L. Stevens, *Simulation of neocortical epileptiform activity using parallel computing*, Neurocomputing **58-60** (2004), 1203–1209.
- [21] W. van Drongelen, H. C. Lee, H. Koch, F. Elsen, M. S. Carroll, M. Hereld, and R. L. Stevens, *Interaction between cellular voltage-sensitive conductance and network parameters in a model of neocortex can generate epileptiform bursting*, Annual International Conference of the IEEE Engineering in Medicine and Biology - Proceedings, 2004, pp. 4003–4005.
- [22] S. A. van Gils, S. G. Janssens, Yu. A. Kuznetsov, and S. Visser, *On local bifurcations in neural field models with transmission delays*, J. Math. Biol. to appear (2012), 1–51.
- [23] R. W. Williams and K. Herrup, *The control of neuron number*, Annual Review of Neuroscience **11** (1988), 423–453.
- [24] H. R. Wilson and J. D. Cowan, *Excitatory and inhibitory interactions in localized populations of model neurons*, Biophys. J. **12** (1972), 1–24.
- [25] ———, *A mathematical theory of the functional dynamics of cortical and thalamic nervous tissue*, Kybernetik **13** (1973), 55–80.